(Received 21 November 2024, Accepted 9 January 2025, Scheduled 31 January 2025)

Ultra-Miniaturized Spiral Antenna for Loop Recorder Implantable Device

Marwah M. Hassooni[1, 3, *], Jabir S. Aziz[2], and Ashwaq Q. Hameed[1]

[1] *Electrical Engineering Department, University of Technology — Iraq, Alsina'a street, Baghdad 10066, Iraq*
[2] *Al-Rafidain University College, Baghdad, Iraq*
[3] *Department of Electrical Engineering, College of Engineering, Al-Iraqia University, Baghdad, Iraq*

ABSTRACT: The miniaturization of implantable antenna is one of the significant requirements, especially for those devices implanted under the skin, as it reduces prominent appearance and invasiveness. In this paper, we design, simulate, and implement a spiral resonator-based microstrip antenna utilizing the ISM band (2.4–2.48 GHz). A small size, light weight, and flat type are required for under-skin implantation. The proposed antenna dimensions were optimized for a miniaturized volume of $(3 \times 2.5 \times 0.12)$ mm^3, representing the smallest size for under-skin biomedical applications. This miniaturization is achieved using a spiral-shaped radiator and creating slots in the ground layer. In-vivo measurement parameters, including reflection coefficient, are measured on the suggested antenna, showing a gain of -19.9 dBi and a bandwidth of 90 MHz. Specific Absorption Rate (SAR) is evaluated at 316 W/kg, confirming that the proposed antenna meets the necessary human-use safety criteria.

1. INTRODUCTION

In the past, implanted devices used inductive coupling at frequencies lower than 200 kHz to transmit information between patients and physicians; however, the data rates are sluggish [1]. A wireless connection between an implantable biomedical device and the exterior base station was created, valid through implantable antennas. A fundamental wireless patient observation system is depicted in Fig. 1. Small implanted biomedical devices put within the human body can potentially enhance many people's lives [2]. In biomedical remote sensing, data transmission is permitted between implanted devices and receivers at a specific range [3]. Challenges present in integrating antennas into biomedical devices are related to their performance and location, as the antenna must operate efficiently within the device's design while reducing interference from surrounding materials and biological tissues. Additionally, long-term reliability is essential, as the antenna must survive physiological states without degradation in performance. Ensuring biocompatibility and stability over time is necessary for the antenna's effectiveness in implantable applications.

The application of the proposed antenna is to enhance the functionality of the implantable loop recorder (ILR), also known as insertable cardiac monitor (ICM). The miniaturized antenna reduces the internal volume of the device, facilitating improved communication between the ILR and external monitoring systems. The implantable loop recorder (ILR), ICM, is a subcutaneous device to diagnose heart rhythm disorders. This device is designed to set up a correlation between symptoms and arrhythmias, thereby enabling the identification of the most appropriate therapy for the patient [4]. An implantable loop recorder is surgically inserted under the skin on the chest and may remain in position for three years or more. These gadgets can transmit one's electrocardiogram (ECG) by telephone to a designated centre in a hospital, medical office, or monitoring firm. A staff member gets the electrocardiogram (ECG) "tracing" and delivers it to the healthcare provider. If the tracing reveals an urgent situation, it must go to the emergency department [4]. Many wireless medical devices interact with adjacent receivers linked to landline networks, cellular networks, or broadband internet access [5]. The Federal Communications Commission (FCC) assigned bandwidth in the 402–405 MHz range for radio communication between implanted devices in 1999. Implantable antennas commonly operate within three frequently used frequency ranges, which include Medical Implantable Communication Service (MICS) band ranging from 402 to 405 MHz, Wireless Medical Telemetry Service (WMTS) band ranging from 1.395 to 1.4 GHz, and Industrial, Scientific, and Medical (ISM) bands covering 433 to 434 MHz, 902 to 908 MHz, 2.4 to 2.48 GHz, and 5.715 to 5.875 GHz. Additionally, some regions have approved Ultra-Wideband (UWB) frequency bands for superior transmission from 3.1 to 10.6 GHz [6]. This type of antenna encounters difficulties related to its size, working frequency licensing, biocompatibility, and the variability of tissue dielectric characteristics. These factors might disrupt the antenna's achievement and affect the specific absorption rate (SAR), posing a security concern [7].

Researchers have published several implantable antenna designs for medical applications. Implantable antennas have used planar inverted-F antennas (PIFAs) in their design owing to their advantages [8, 9]. Microstrip antennas have advantages, such as reduced dimensions and decreased weight,

* Corresponding author: Marwah M. Hassooni (hassoonimarwa@gmail.com).

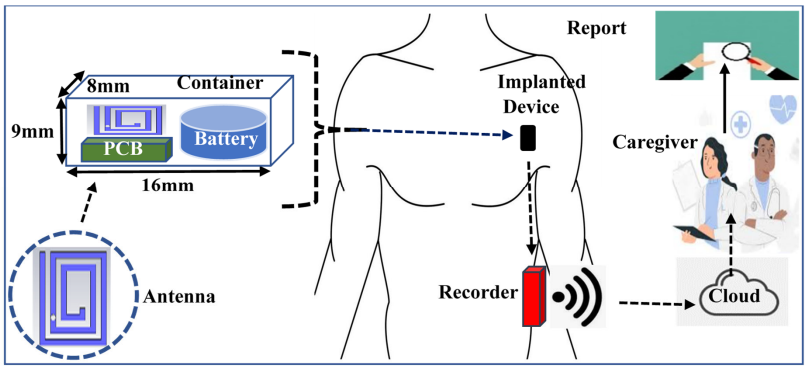

FIGURE 1. Schematic of wireless monitoring utilizing implanted device.

compared to traditional PIFAs antennas. The study in [10] proposes a flexible, biocompatible antenna functioning in ISM band (2.4–2.48 GHz) specifically designed for health-related implants. The antenna, integrated with Polydimethylsiloxane (PDMS), exhibits wide bandwidth characteristic, covering the entire ISM band with a bandwidth of 350 MHz. However, its relatively large dimensions may restrict its immediate applicability in miniaturized biomedical devices. The study in [6] proposes an extremely tiny implanted antenna for wireless cardiac pacemaker devices of $3\,\text{mm} \times 3\,\text{mm} \times 0.5\,\text{mm}$ volume working in the ISM range (2.4–2.48 GHz). The antenna reaches a 22% bandwidth and -24.9 dBi peak gain. While the design succeeds in compactness and fulfills SAR safety criteria, its low gain restricts communication range, and detuning effects in biological contexts may influence long-term performance.

The paper in [11] offers a circularly polarized implantable antenna that operates in two frequency bands for biomedical communication in ISM bands (0.915 GHz and 2.4 GHz). The antenna has a bandwidth axial ratio of 220 MHz at 0.915 GHz and 230 MHz at 2.45 GHz, showing the highest gains of -29.5 dBi and -19.2 dBi, respectively; the miniature dimensions of 61.7 mm^3 are attained by using T-shaped slots and a short-circuit probe. In [12], the authors present a miniaturized antenna for leadless pacemakers, achieving an impressive ultra-wide bandwidth of 3380 MHz; however, they reported high gain values. The research in [13] extensively examines a tiny tri-band implantable antenna, showcasing a small volume of 75 mm^3 and bandwidths of 181.8% at 0.86, 9.58% for 1.43 GHz and 285.7% for UWB/Wi-Fi frequencies. A tiny dual-band antenna featuring circular polarization (CP) feature for a wireless capsule imaging system device with a size of 2.11 mm^3 is presented in [14]. Still, this antenna has a narrow bandwidth that causes frequency shifts. A circularly polarized wideband patch antenna for continuous glucose level tracking devices was created in a recent paper [15]. This design produces a simulated bandwidth of 1.1 GHz (1.65–2.75 GHz) while working in the mid-field band (1.9 GHz) and ISM band (2.45 GHz). The antenna exhibits a gain of -20.04 dBi at 2.45 GHz and -24.64 dBi at 1.9 GHz. This study introduces the characterization and design of a small antenna for under-skin implantation devices. The designed antenna is optimized for operation at standard biomedical frequencies and is considered the smallest realized antenna for under-skin medical applications, achieving excellent gain compared to currently available solutions. In order to make an assessment, Table 1 compares the characteristics and attributes of previously submitted papers with the suggested antenna.

2. THEORETICAL BACKGROUND

The human body's challenging and changeable nature has various difficulties for wireless transmission. Human bodies comprise many tissues containing skin, fat, muscles, and bones, each with a distinct electrical conductivity and permittivity that can change owing to various aspects, encompassing age, weight gain or loss, and posture [26].

There is a large variety of device sizes and alterations in Implanted Medical Devices (IMDs) design and area. The size of an implanted implant medical device (IMD) is carefully chosen to ensure that it can accomplish its intended duties. However, the frequency of the implanted antenna may detune from its authorized working frequencies owing to a variety of traits, including the complexity of the human body and possible changes in close environments. Regardless of the implantation scenarios, a microstrip patch implanted antenna with a miniaturized size is proposed for implanted medical systems in this study. The first estimation for the configuration of the implantable antenna, aimed at a designated frequency of 2.4 GHz, was based on the equation utilized in [27].

$$f_r = \frac{c}{\lambda_g \sqrt{\varepsilon_{eff}}} \approx \frac{c}{L_g \sqrt{\frac{\varepsilon_r}{2}}} \tag{1}$$

where c, λ_g, f_r, and ε_{eff} indicate the speed of the electromagnetic (EM) waves in free space guiding the wavelength, resonance frequency in addition to free space, and effective permittivity, respectively. Likewise, L_g represents the length of the antenna where "ε_r" is the substrate's united relative dielectric constant. The superstrate layer was mainly used to prevent the antenna's radiator from directly contacting human flesh, thereby isolating the antenna from the lossy environment [27, 28]. However, in our design, the antenna was encapsulated and simulated inside a dummy system to make it more realistic without a superstrate. Typically, the layer called a superstrate with a high dielectric constant used to decrease

TABLE 1. Comparison of the characteristics and attributes of previously submitted papers with the suggested antenna.

Ref.	Year	Freq. GHz	Dimension mm^3	$SAR_{1g,max}$ W/kg	$Gain_{max}$ [dBi]	10dB-BW MHz	Shorting Pin	Superstrate
[2]	2019	0.928 2.45	7 ×7 × 0.2	471 313	-28.44 -25.65	184.1 219.7	Yes	Yes
[16]	2019	0.402 1.60 2.45	7 × 6.5 × 0.377	588 441 305	-30.5 -22.6 -18.2	148 171 219	No	yes
[14]	2020	0.915 2.450	6.5 × 6.5 × 0.05	420.3 233.2	-28.2 -24.5	26 50	No	yes
[17]	2021	2.45	7 × 7 × 0.2	350.81	-15.8	1533	Yes	Yes
[18]	2021	2.4	3 × 4 × 0.5	270.28	-25.95	525	No	yes
[19]	2022	1.4 2.45	6 × 6 × 0.254	256.9 142.6	− 32.7 − 25.92	250 430	No	No
[20]	2022	0.400 2.4 5.7	3.04 ×10 ×17.25	308 292 328	-40 -15 -13.5	53 237 350	Yes	Yes
[21]	2023	2.4, 4.8 5.8	9.2 × 9.2 × 0.5	97.9, 205, 156	− 15.2 -16.6, - 15.8	150, 75, 200	No	Yes
[22]	2023	2.45, 5.8	3.4 × 6.6 × 0.254	263.3 107.45	− 31.6, − 21.4	1,050, 1,900	No	No
[23]	2024	1.4 2.45	8.2 × 8.2 × 0.635	84.8 123.7	−29.4 −30.4	-	Yes	Yes
[24]	2024	0.915 2.4	6 × 6 × 0.25	891 877	−21.8 −19.2	120 310	No	No
[15]	2024	2.45	6.59 × 6.59 × 0.61	463	−20.04	1100	2	Yes
[25]	2024	0.915, 1.400, 2.450	6 × 7 × 0.127	-	− 25.73, − 18.56, − 15.33	3040	-	-
This work	2024	2.45	3 × 2.5 × 0.12	316	-19.9	90	No	No

the actual antenna size [29]. Additionally, the effect of "ε_r" on the wavelength (λ) of an electromagnetic wave facilitates the process of miniaturization. The value of λ may be determined in the absence of any external influences. The value of λ could be calculated in the free-space using

$$\lambda = \frac{c}{f_r} \tag{2}$$

Nevertheless, in a non-free space environment, the value of λ is reduced owing to the high permittivity values, as shown by equation [17]. High permittivity is very beneficial when implantable antennas are designed since miniaturization is an important consideration. As a result, the designed antenna was successfully miniaturized, with an overall volume of only 0.9 mm^3.

The achievement makes the small antenna capable of maintaining a proper impedance match. A tissue model used in the study thoroughly represented the complicated biological environment surrounding the implanted system. A model took into account various variables, including tissue composition, electrical conductivity, permittivity, and anatomical geometry. By incorporating these parameters into the model, the researchers could accurately simulate the behaviour and interaction of implanted devices within the specific tissue environment [30]. Hence, a detailed tissue model is essential in evaluating system performance and potential effects on surrounding tissues, then optimising the implanted devices' design and functionality [31].

The choice of tissue model relies on the specific research purposes, prepared data, and the detail required for the simulation. They often select the most appropriate type of tissue model to accurately represent the tissue environment and facilitate realistic simulations of implanted devices. Identical tissue model considers tissues as having consistent electrical properties and composition, a more actual representation of the tissue structure called the layered tissue model or heterogeneous tissue model, which takes into account the nonuniform distribution of electrical properties. The composition across different tissue regions provides a more specified representation of the tissue environment [32].

3. ANTENNA GEOMETRY

The construction of the suggested radiator is shown in Fig. 2(a), which contains a spiral component and a necessary layout. As indicated in Fig. 2(b), three rectangular slots are made in the ground layer to improve bandwidth and adjust the resonant frequency. Fig. 2(c) illustrates the side view of the antenna, which is essential for understanding its design and functionality. High dielectric substrate material (Rogers RO3010, $\varepsilon_r = 10.2$, $\tan\delta = 0.0022$) has a thickness of 0.12 mm and is used for downsizing. As the insulating material for encasing,

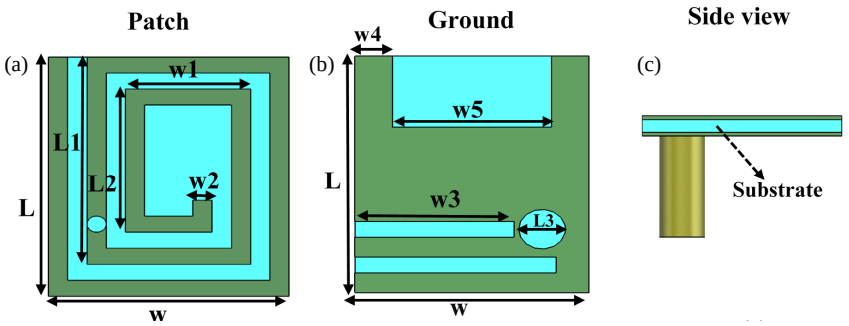

FIGURE 2. The configuration of the proposed antenna. (a) Form of radiator plan structure. (b) Ground plan. (c) Side view.

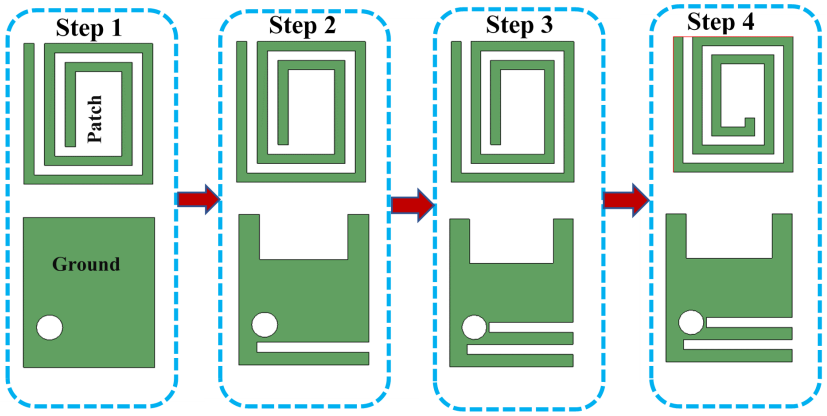

FIGURE 3. The antenna design procedure included developing a tiny MPA antenna.

TABLE 2. All the specifications of the proposed antenna.

Variable	Value mm	Variable	Value mm
L	3	W1	1.3
W	2.5	W2	0.2
L1	2.6	W3	1.7
L2	1.8	W4	0.4
L3	0.5	W5	1.7

a biocompatible 0.2-mm-thick acrylic ($\varepsilon_r = 4$) is used. The antenna that is shown has a small volume of 0.9 mm^3. Table 2 presents all the parameters of the suggested antenna design.

As depicted in Fig. 3, the suggested model of the antenna was developed in four stages starting with the development of a standard radiator and ground plane. Since one downsizing approach that may lower the resonance frequency is current path lengthening [10], meandering and spiral line patches have been proposed.

Because the spiral construction has improved radiation efficiency and has a lower resonance frequency than a meandering antenna of the same physical length, we selected it [11]. The spiral antenna structure incorporates a rectangular radiator and a slot in the ground layer with a line width of 0.2 mm. Initially, without any modifications, which is a foundation for further modifications and optimizations, the antenna resonates at approximately 1.1 GHz and 3.49 GHz (step 1).

Slots are incorporated into the ground plane to shift the resonant frequency. This modification causes the operating frequency shifted to the lower frequency to 0.825 GHz and 2.8 GHz, respectively. Notably, the second resonance is close to 2.4 GHz (step 2), a desired frequency range for many wireless communication applications.

In the next step, further optimization occurs. Here, we insert a third slot into the ground plane. This addition adjustment shifts the resonant operating frequency towards a lower range, creating dual resonant frequencies at 0.82/2.7 GHz (step 3), allowing for increased flexibility when the required frequency band is selected for particular communication applications and specifications.

Finally, the spiral radiator length is increased to obtain the resonance at 2.4 GHz (step 4) while ensuring proper matching, and this step represents the most refined version of the antenna. That tuning enables the antenna to resonate suitably at the desired frequency. This step makes it suitable for applications that rely on the 2.4 GHz frequency spectrum, such as Bluetooth and wireless connectivity.

Through achieving all these adjustments, the spiral-shaped antenna structure can be designed to operate within specific frequency ranges of interest. This modification is beneficial for various wireless-dependent applications where accurate frequency tuning is required to ensure optimal achievement and compatibility with existing communication systems. 0.5 mm represents the range from the feed position to the edge of the radiator.

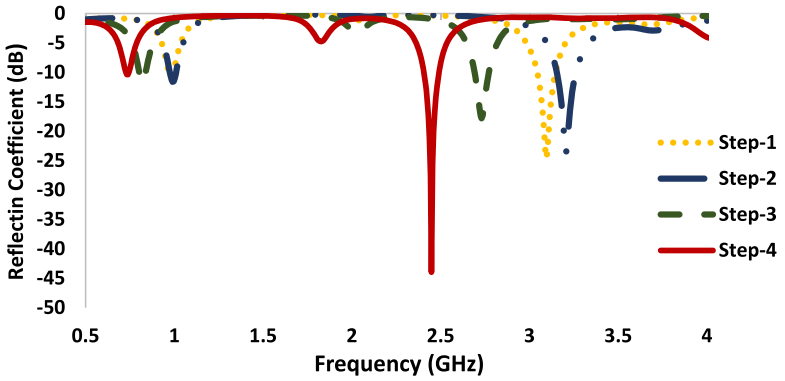

FIGURE 4. Reflection coefficient (S_{11}) for each of the four successive phases of the proposed antenna (Steps 1–4).

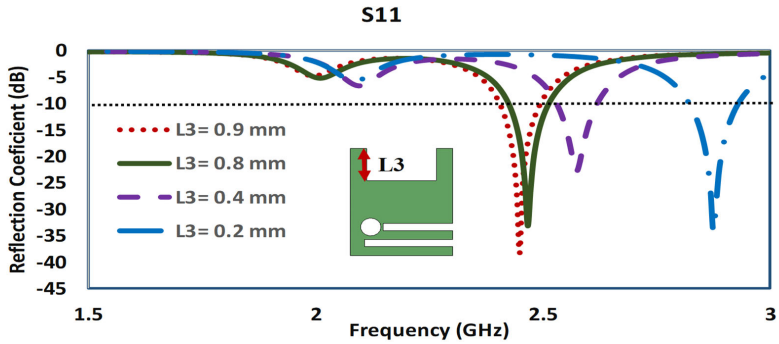

FIGURE 5. Influence of variations in $L3$ on S_{11}.

Figure 4 illustrates the changes in S_{11} over four successive design phases. During these phases, components, the size of the patch, and all other model layers remain unchanged. The step-by-step method lets us try different combinations in a planned way, ensuring that the end design meets the requirements for use. We used a high-performance 3D EM analysis software package (CST) to model, simulate, and analyze the implantable and integrated antenna systems.

3.1. Parametric Study of the Model

The optimization of the antenna and the selection of optimal parameter dimensions based on the specific scenario are determined through a parametric analysis of the antenna. The suggested antenna was maintained at the homogeneous skin phantom homogeneous skin phantom (HSP) to investigate how changes in its properties might affect S_{11}. The critical design parameters for the proposed spiral antenna for the parametric study are $L3, W5$ lengths and feeding position.

3.1.1. Effect of Varying of Open-End Slots Length L3

Figure 5 illustrates the effect of varying the open-ended slots ($L3$) length, ranging from 0.2 mm to 0.9 mm. Decreasing $L3$ results in a shift of the S_{11} curve towards higher frequencies. Precisely, for $L3 = 0.2$ mm, the resonant frequency shifts from the desired 2.45 GHz and instead resonates around 2.8 GHz. This behaviour suggests that to achieve resonance at 2.45 GHz, a more considerable value of $L3$ (such as 0.8 mm or 0.9 mm) would be more appropriate, as these dimensions yield resonant frequencies closer to the target value.

3.1.2. Effects of Feed Position Variation

The influence of feeding variations position on the S_{11} is visualized in Fig. 6. Position 1 shows a significant dip around 2.45 GHz, indicating suitable impedance matching with values around -39 dB or lower, suggesting efficient signal transmission. In contrast, position 2 exhibits a less pronounced dip at this frequency, indicating poorer matching and increased reflection. Position 3 has S_{11} values (less negative) at 720 MHz, suggesting that it is the least effective in terms of impedance matching, leading to significant signal loss.

3.1.3. Effect of Varying of W5 on the S_{11}

Figure 7 illustrates the impact of varying the width ($W5$) on the reflection coefficient (S_{11}). As $W5$ increases from 0.5 mm to 1.7 mm, the reflection coefficient shifts to lower frequencies. Specifically, with $W5 = 0.5$ mm, the proposed antenna resonates at 2.61 GHz. When $W5$ increases to 0.9 mm, the resonance frequency turns to 2.52 GHz. Notably, $W5 = 1.7$ mm demonstrates the best performance due to its S_{11} value, indicating optimal impedance matching. Conversely, $W5 = 0.5$ mm shows less matching, emphasizing that wider widths yield better resonance and matching for medical applications. Wider widths tend to concentrate the current flow, leading to better impedance matching and lower resonant frequencies.

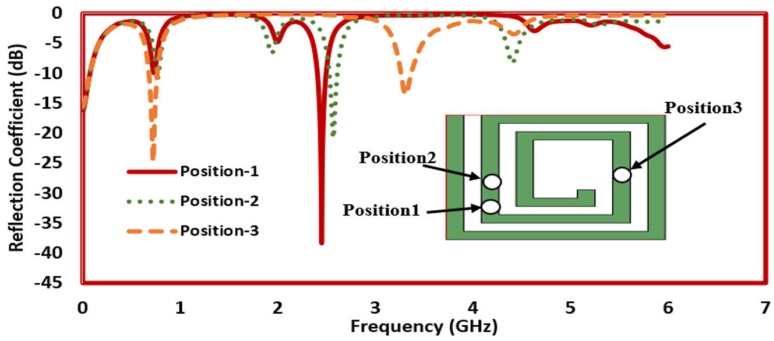

FIGURE 6. Impact of changes in feed position on S_{11}.

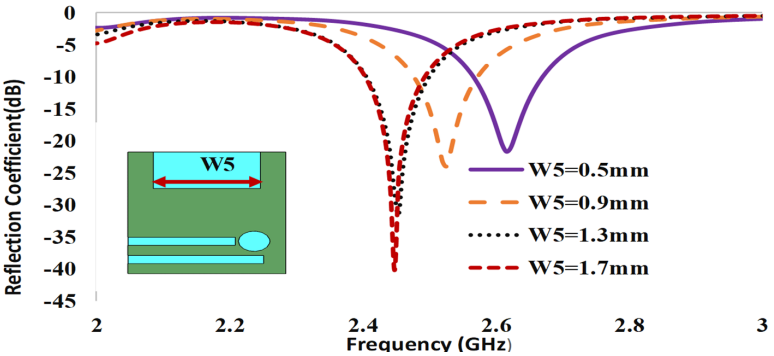

FIGURE 7. Effect of varying of $W5$ on the S_{11}.

3.2. Encapsulation of Microstrip Antenna

A miniaturized and efficient microstrip antenna has been designed for under-skin devices encapsulated by a 9 mm × 16 mm × 8 mm container. The antenna is incorporated with the components as a dummy system to ensure optimal performance within a realistic medical device context and reveal insights into its performance characteristics when being incorporated into an actual implanted device, as shown in Fig. 1. For encapsulation, we chose a biocompatible 0.2 mm thick acrylic material. Rogers material was used to mimic the printed circuit board (PCB) inside the container

3.3. Tissue Prototype

The performance of an implantable antenna, whether it remains fixed or moves within human organs (e.g., glucose monitoring, drug delivery, and pacemaker), can be affected by the presence of nearby lossy media and the interface between adjacent tissues and the antenna's near field. This close interface between the antenna and surrounding biological environment has the potential to alter the antenna's functionality and performance characteristics. Two scenarios, one-layer phantom and heterogenous phantoms, were used for validation purposes to evaluate the effectiveness of antennas in various media situations. A rectangular cuboid phantom with (80 mm × 80 mm × 15 mm) dimensions has been used for skin phantom and heterogenous cuboid phantom of three skin, fat, and muscle layers with (80 mm×80 mm×29 mm) dimensions. The antenna is mounted 9 mm under the Cutaneous layer of HSP and 8 mm in heterogeneous phantom. CST software has been used to simulate this model, as depicted in Fig. 8.

3.4. Current Distributions

Figure 9 shows the proposed antenna's current distributions at resonant frequencies. It is implied and confirmed by the current distribution that the operating frequency is reciprocally proportional to the effective area of the microstrip antenna. The patch plane ultimately radiates in the 2.45 GHz band, as illustrated in Fig. 9(a). As one can see, the surface current movement is in a similar direction to the spiral's outer ring, and the current flow is constant.

3.5. Consideration of SAR

Specific Absorption Rate (SAR) is a method employed to calculate the energy absorption rate in the human body [16]. Additionally, it measures radiation absorption per unit mass of human tissue and power deposition and is defined by the equation below [17, 18].

$$\text{SAR} = \frac{\sigma E^2}{2\rho} \tag{3}$$

where E is the magnitude of the electric field, and σ and ρ are the conductivity and mass density of the biological tissue, respectively. SAR must not exceed 1.6 W/kg over-averaged for any 1-g cubic tissue specified by IEEE C95.1-1999 regulations to adhere to safety rules [19]. It should not exceed 2 W/kg per 10 g, according to IEEE C95.1-2005.

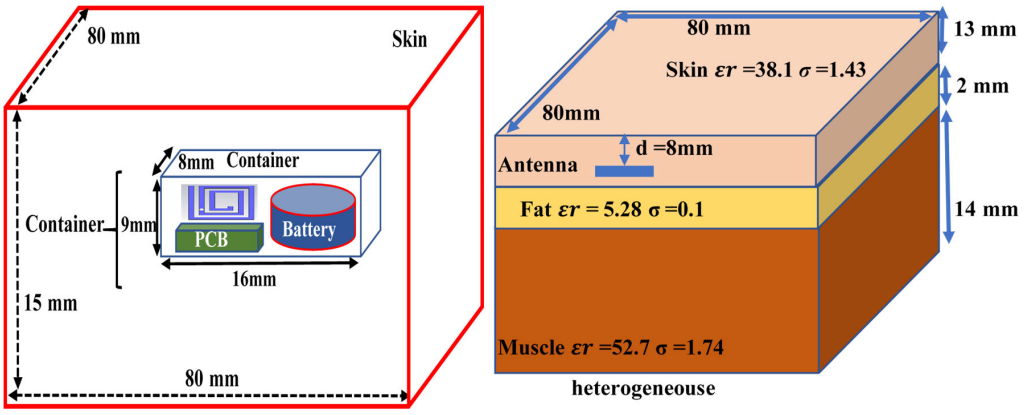

FIGURE 8. Simulation of the antenna into a one-layered homogeneous and heterogeneous body model.

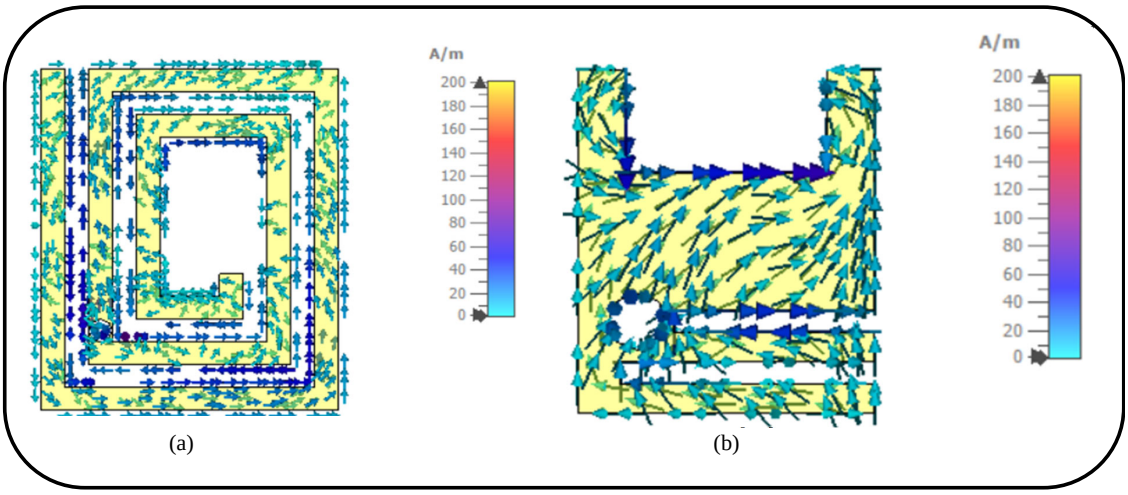

FIGURE 9. The current allocation of the proposed antenna at 2.4 GHz. (a) Patch. (b) Ground.

TABLE 3. Maximal value of specific absorption rate for 1 watt of input power and permitted maximal input powers.

Frequency (GHz)	Tissue structure	Specific Absorption Rate (W/kg)		Maximum provided input power (mW)	
		1 g-Avg	10 g-Avg	1 g-Avg	10 g-Avg
2.45 GHz	Skin	316	32.1	5.06	62.3

The calculation of SAR values using a homogeneous skin phantom, characterized by a dielectric constant of 38 and a conductivity of 1.47 S/m to represent skin properties, involves modeling electromagnetic field interactions within a uniform medium that maintains consistent electrical properties across the model. The SAR is determined by analyzing the electric field distribution within the phantom by applying the formula (2). Table 3 illustrates the SAR values obtained at a frequency of 2.45 GHz. When the input power is held at 1 W, the specific absorption rate (SAR) values for the 1 g and 10 g standards are 316 and 32.1 W/kg, respectively. Based on these values, we are able to determine that the maximum amount of allowable power needed to meet the protection standard of 1.6 W/kg for a specific absorption rate of 1 g is 5.06 milliwatts. However, to ensure that 10 g of SAR does not exceed the safety limit of 2 W/kg, it is necessary to consider an output power of 62.3 mW. These values satisfy the SAR requirements. The SAR value has been assessed and depicted in Fig. 10.

3.6. Radiation Patterns

Figure 11 illustrates the antenna's radiation patterns in a homogeneous environment of a skin model at 2.450 GHz frequency. The pattern is primarily symmetric; however, the Phi $= 90°$ plane exhibits enhanced radiation with more prominent lobes, signifying more gain than Phi $= 0°$. Specific nulls in the Phi $= 0°$ plane indicate regions of reduced radiation. Although

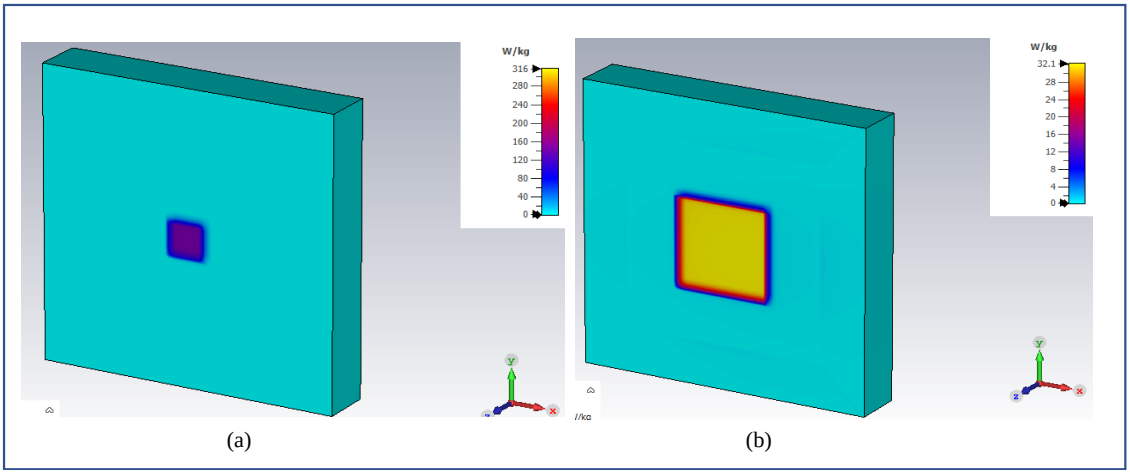

FIGURE 10. The SAR is resolved by modeling the cuboid homogenous phantom. (a) Specific Absorption Rate (SAR) of 1 g of tissue at a frequency of 2.45 GHz. (b) Specific Absorption Rate (SAR) of 10 g of tissue at a frequency of 2.45 GHz.

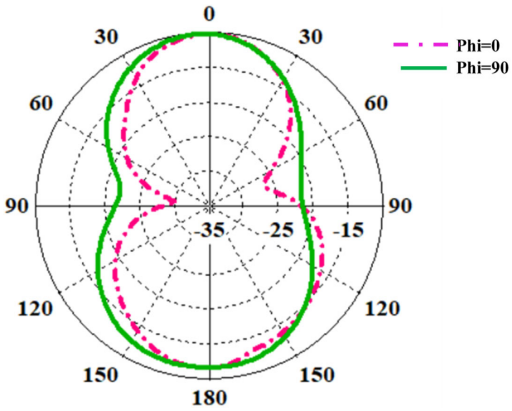

FIGURE 11. Simulated radiation patterns at 2.45 GHz.

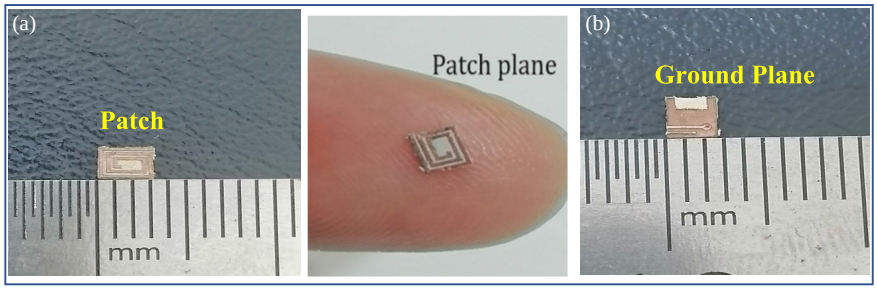

FIGURE 12. Fabricated microstrip implantable antenna. (a) Radiator plane. (b) Ground plane.

the Phi $= 90^{\circ}$ pattern has a smoother appearance, it means a more even power distribution. These attributes are characteristics of a spiral antenna, recognized for its broad bandwidth and consistent emission at several angles, rendering it appropriate for biomedical implants where orientation stability is paramount.

The suggested antenna optimum gain at the 2.45 GHz frequency was -19.9 dBi in the homogenized phantom, and implant antenna efficiency decreased due to the requirement for miniaturization [19].

4. IMPLEMENTATION AND EXPERIMENTAL SETUP

The proposed implanted microstrip antenna is constructed on a PCB using a Rogers RO3010 substrate, as shown in Fig. 12. The entire antenna size is $3\times2.5\times0.12\,\text{mm}^3$. Etching technique was used to fabricate the radiator and ground layer on the substrate. The system container dimension ($9\,\text{mm}\times16\,\text{mm}\times8\,\text{mm}$) is manufactured using acrylic material. The system container, antenna model, and assessment setup are shown in Fig. 13. Additionally, the S-parameters of the antenna are determined by placing the system container within cow meat.

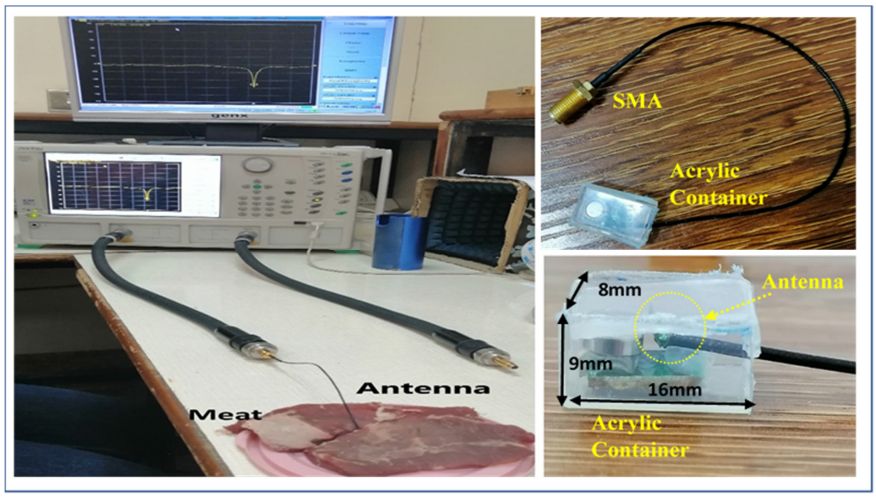

FIGURE 13. Measured S_{11} parameters of the proposed antenna and testing environment.

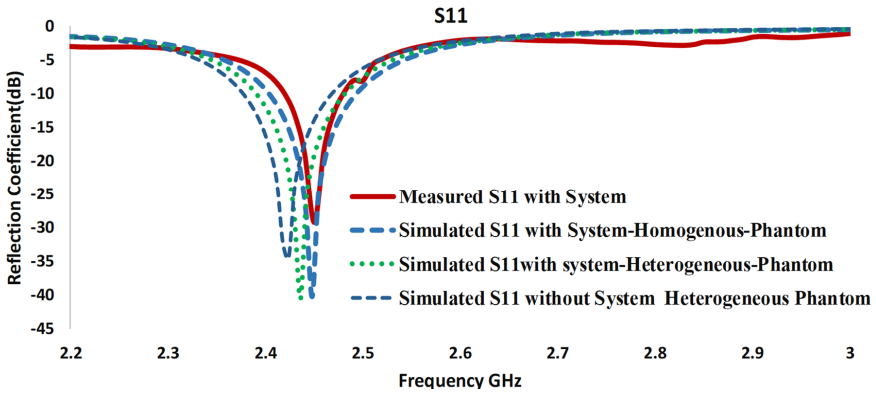

FIGURE 14. Comparison of the simulated and measured S_{11}-parameters of the suggested antenna.

5. MEASUREMENTS AND RESULTS

The antenna system under consideration was first simulated using homogeneous skin phantoms corresponding to the implanted device located under the skin, as shown in Fig. 8. The fabrication and testing of this antenna have been performed. The implanted device is put within beef to measure S-parameters. Fig. 14 displays the comparison of the S-parameters measured with the acrylic container. The results indicate that the antenna maintains its operational efficiency regardless of the inclusion of the system. The design is robust enough to withstand variations in different scenarios. The measured S_{11} has a bandwidth of 90 MHz (2.40–2.493 GHz) with a 10 dB range and a resonant frequency of 2.45 GHz. The results of constructed models show a strong correlation.

6. CONCLUSION

In this communication, an implantable microstrip antenna designed for the 2.4 GHz ISM frequency range offers valuable recommendations for observation utilizations. The single-band implantable antenna is chosen for communication with the loop recorder because it is optimized for efficiency at a specific frequency, ensuring reliable signal transmission with minimal energy consumption. An antenna system is built through dummy electrical components and an implanted antenna. The antenna's open-ended slots benefit frequency adjusting, miniaturization, and impedance matching in the ground plane. A significantly reduced size of 3 mm $\times$ 2.5 mm $\times$ 0.12 mm was accomplished for the suggested antenna because of the use of a high value of dielectric substrate and spiral radiation patch without superstrate and shorting pins; it might cause difficulties for the real implementation. Examining the prototypes of an incorporated antenna system in the Cow muscle confirmed the validity of the results. Furthermore, the suggested antenna met the safety criteria of International Commission on Non-Ionizing Radiation Protection (ICNIRP) and IEEE C95.1-1999. Due to its improved performance and compact volume, the suggested spiral microstrip antenna has the potential to be an excellent choice for contemporary technology in implanted loop recorder medical systems.

REFERENCES

[1] Halperin, D., T. S. Heydt-Benjamin, B. Ransford, S. S. Clark, B. Defend, W. Morgan, K. Fu, T. Kohno, and W. H. Maisel, "Pacemakers and implantable cardiac defibrillators: Software radio attacks and zero-power defenses," in *2008 IEEE Symposium*

on Security and Privacy, 129–142, Oakland, CA, USA, 2008.

[2] Faisal, F. and H. Yoo, "A miniaturized novel-shape dual-band antenna for implantable applications," *IEEE Transactions on Antennas and Propagation*, Vol. 67, No. 2, 774–783, Feb. 2019.

[3] Huang, S.-M., M.-R. Tofighi, and A. Rosen, "Considerations for the design and placement of implantable annular slot antennas for intracranial pressure monitoring devices," *IEEE Antennas and Wireless Propagation Letters*, Vol. 14, 1514–1517, 2014.

[4] Bisignani, A., S. D. Bonis, L. Mancuso, G. Ceravolo, and G. Bisignani, "Implantable loop recorder in clinical practice," *Journal of Arrhythmia*, Vol. 35, No. 1, 25–32, 2019.

[5] Mahn, T. G. and K. A. Barritt, "Wireless medical technologies: Navigating government regulation in the new medical age," Fish's Regulatory & Government Affairs Group, 2013.

[6] Feng, Y., Z. Li, L. Qi, W. Shen, and G. Li, "A compact and miniaturized implantable antenna for ISM band in wireless cardiac pacemaker system," *Scientific Reports*, Vol. 12, No. 1, 238, 2022.

[7] Zada, M. and H. Yoo, "A miniaturized triple-band implantable antenna system for bio-telemetry applications," *IEEE Transactions on Antennas and Propagation*, Vol. 66, No. 12, 7378–7382, Dec. 2018.

[8] Huang, Z., H. Wu, S. S. Mahmoud, and Q. Fang, "Design of a novel compact MICS band PIFA antenna for implantable biotelemetry applications," *Sensors*, Vol. 22, No. 21, 8182, 2022.

[9] Kumar, R. and S. Singh, "CPW-fed conformal PIFA design for implantable IoMT devices with wideband performance," *IEEE Sensors Journal*, Vol. 24, No. 1, 231–237, 2024.

[10] Scarpello, M. L., D. Kurup, H. Rogier, D. V. Ginste, F. Axisa, J. Vanfleteren, W. Joseph, L. Martens, and G. Vermeeren, "Design of an implantable slot dipole conformal flexible antenna for biomedical applications," *IEEE Transactions on Antennas and Propagation*, Vol. 59, No. 10, 3556–3564, 2011.

[11] Song, Z., X. Xu, Y. Wang, Y. Shi, X. Zheng, and L. Wang, "Design of a miniaturized dual circularly polarized implantable antenna by using characteristic mode method," *Scientific Reports*, Vol. 14, No. 1, 16384, 2024.

[12] Alghamdi, A., A. Alshammari, L. Chang, A. Iqbal, and I. B. Mabrouk, "Miniaturized implantable antenna with ultra-wide bandwidth characteristics for leadless pacemakers," in *2024 18th European Conference on Antennas and Propagation (EuCAP)*, 1–5, Glasgow, United Kingdom, 2024.

[13] Gupta, A., V. Kumar, S. Bansal, M. H. Alsharif, A. Jahid, and H.-S. Cho, "A miniaturized tri-band implantable antenna for ISM/WMTS/Lower UWB/Wi-Fi frequencies," *Sensors*, Vol. 23, No. 15, 6989, 2023.

[14] Hayat, S., S. A. A. Shah, and H. Yoo, "Miniaturized dual-band circularly polarized implantable antenna for capsule endoscopic system," *IEEE Transactions on Antennas and Propagation*, Vol. 69, No. 4, 1885–1895, Apr. 2021.

[15] Song, Z. and M. Li, "Ultra-wideband circular polarized implantable patch antenna for implantable blood glucose detection system applications," *Sensors*, Vol. 24, No. 16, 5292, 2024.

[16] Shah, I. A., M. Zada, and H. Yoo, "Design and analysis of a compact-sized multiband spiral-shaped implantable antenna for scalp implantable and leadless pacemaker systems," *IEEE Transactions on Antennas and Propagation*, Vol. 67, No. 6, 4230–4234, 2019.

[17] Yousaf, M., I. B. Mabrouk, M. Zada, A. Akram, Y. Amin, M. Nedil, and H. Yoo, "An ultra-miniaturized antenna with ultra-wide bandwidth characteristics for medical implant systems," *IEEE Access*, Vol. 9, 40 086–40 097, 2021.

[18] Zada, M., I. A. Shah, A. Basir, and H. Yoo, "Ultra-compact implantable antenna with enhanced performance for leadless cardiac pacemaker system," *IEEE Transactions on Antennas and Propagation*, Vol. 69, No. 2, 1152–1157, Feb. 2021.

[19] Sharma, D., B. K. Kanaujia, V. Kaim, R. Mittra, R. K. Arya, and L. Matekovits, "Design and implementation of compact dual-band conformal antenna for leadless cardiac pacemaker system," *Scientific Reports*, Vol. 12, No. 1, 3165, 2022.

[20] Shahverdi, K., S. Hashemi, S. Sarafan, and H. Cao, "Triple-band implantable antenna design for biotelemetry applications in MICS/ISM/Wi-Fi/Bluetooth bands," *Technologies*, Vol. 10, No. 4, 91, 2022.

[21] Mosavinejad, S. S., P. Rezaei, A. A. Khazaei, and J. Shirazi, "A triple-band spiral-shaped antenna for high data rate fully passive implantable devices," *AEU — International Journal of Electronics and Communications*, Vol. 159, 154474, 2023.

[22] Sharma, D., B. K. Kanaujia, S. Kumar, K. Rambabu, and L. Matekovits, "Low-loss MIMO antenna wireless communication system for 5G cardiac pacemakers," *Scientific Reports*, Vol. 13, No. 1, 9557, 2023.

[23] Alshammari, A., A. Iqbal, A. Basir, R. B. V. B. Simorangkir, and I. B. Mabrouk, "Ultra-miniaturized dual-band implantable antenna for wireless capsule endoscopy," *IEEE Sensors Journal*, Vol. 24, No. 9, 15 210–15 218, 2024.

[24] Lamkaddem, A., A. E. Yousfi, V. González-Posadas, and D. Segovia-Vargas, "Miniaturized dual band implantable antenna for implanted biomedical devices," *IEEE Access*, Vol. 12, 15 026–15 036, 2024.

[25] Faisal, F., A. Moulay, M. Chaker, and T. Djerafi, "Efficient wireless power transfer to an ultra-miniaturized antenna for future cardiac leadless pacemaker," in *2024 18th European Conference on Antennas and Propagation (EuCAP)*, 1–4, Glasgow, United Kingdom, 2024.

[26] Brandão, P. and J. Bacon, "Body sensor networks: Can we use them?" in *Proceedings of the International Workshop on Middleware for Pervasive Mobile and Embedded Computing*, 1–6, New York, NY, USA, 2009.

[27] Das, S. and D. Mitra, "A compact wideband flexible implantable slot antenna design with enhanced gain," *IEEE Transactions on Antennas and Propagation*, Vol. 66, No. 8, 4309–4314, 2018.

[28] Xu, L.-J., Y.-X. Guo, and W. Wu, "Bandwidth enhancement of an implantable antenna," *IEEE Antennas and Wireless Propagation Letters*, Vol. 14, 1510–1513, 2014.

[29] Lin, H.-Y., M. Takahashi, K. Saito, and K. Ito, "Performance of implantable folded dipole antenna for in-body wireless communication," *IEEE Transactions on Antennas and Propagation*, Vol. 61, No. 3, 1363–1370, 2013.

[30] Soliman, M. M., M. E. H. Chowdhury, A. Khandakar, M. T. Islam, Y. Qiblawey, F. Musharavati, and E. Z. Nezhad, "Review on medical implantable antenna technology and imminent research challenges," *Sensors*, Vol. 21, No. 9, 3163, May 2021.

[31] Arora, G., P. Maman, A. Sharma, N. Verma, and V. Puri, "Systemic overview of microstrip patch antenna's for different biomedical applications," *Advanced Pharmaceutical Bulletin*, Vol. 11, No. 3, 439–449, 2021.

[32] Damaj, A. W., H. M. E. Misilmani, and S. A. Chahine, "Implantable antennas for biomedical applications: An overview on alternative antenna design methods and challenges," in *2018 International Conference on High Performance Computing & Simulation (HPCS)*, 31–37, Orleans, France, 2018.